Modelling liquefaction of soils with LS-DYNA using a SANISAND-based material model

Richard Sturt[1], Cihan Cengiz[1], Yuli Huang[2], James Go[1], Samila Bandara[1], Anton Pillai[1]

[1]Arup, UK
[2]Formerly Arup, USA

1   Abstract

Saturated sandy soils can be prone to liquefaction during earthquakes: the soil loses strength and stiffness due to cyclic shear loading, becoming more like a liquid or quicksand. When liquefaction occurs, structures founded on such soils may experience severe damage or large settlement, or may even overturn. Designers of structures in seismically-active regions where liquefiable soils are present need to assess the likelihood of liquefaction occurring under design-level earthquakes and, if required, provide mitigating measures in the design. Three-dimensional nonlinear finite element analysis can be used to understand the effects of liquefaction on a structure and, if sufficient validation of the soil properties has been carried out under a range of stress conditions, can potentially predict the extent of liquefaction that will occur as a result of a given earthquake time-history. However, this requires a soil material model capable of reproducing the phenomena relevant to liquefaction.

LS-DYNA already has extensive capabilities for modelling structures, soils and soil-structure interaction, together with the ability to process large 3D models quickly. It is therefore potentially an ideal simulation tool for modelling the effects of liquefaction on structures during engineering design projects. The principal obstacle until now has been the lack of a liquefaction-capable soil material model.

This paper describes the liquefaction phenomenon and shows the potential of LS-DYNA to model it. A material model has been developed based on SANISAND, which is a family of soil models in the framework of critical state soil mechanics and bounding surface plasticity that has become well-established in the academic community over the last two decades for purposes of modelling liquefaction. Results are compared against a shake table test using a laminar shear box, and an example is given of application to engineering design.

2   Introduction

Liquefaction is a temporary loss of stiffness and strength that can occur in saturated sandy soils during earthquakes. The soil becomes like a liquid or quicksand and may exhibit very large deformations. Structures relying on support by such soils can be severely damaged.

2.1   Impacts of liquefaction

Soil liquefaction is a major contributor to seismically induced damage on infrastructure including soil structures (dams), linear infrastructure (lifelines), building foundations, and coastal structures. For instance, in the 1990 Luzon Earthquake with a magnitude of 7.8, liquefaction phenomena have caused extensive damage to buildings' foundations where structural integrity has been compromised and lives were lost [1]. Similarly, liquefying soils are responsible for significant damage to marine structures such as quay walls and gantry cranes in the 1999 Kocaeli earthquake (Mw=7.6) [2]. Perhaps the seismic event with the most disastrous liquefaction induced consequences is the 1964 Niigata Earthquake where significant damage was registered on bridges, airports, and apartment buildings with large economic losses. Figure 1 illustrates the failure pattern inflicted by liquefaction on a block of flats in Niigata. Recently, the Canterbury earthquake sequence (2010-2011) and 2011 Tohoku earthquake have also caused extensive damage to structures and their foundation systems. Typical liquefaction induced damage patterns include the following:
- Lateral flow/spreading of embankments and earth dams;
- Excessive differential settlements of buildings foundations triggering collapse;
- Damage to linear infrastructure such as pipelines, roads, and railways

Fig.1:   Collapse of apartment blocks caused by liquefaction in the 1964 Niigata earthquake

The scarcity of suitable land for urbanization is pushing more and more people to live in earthquake prone areas. According to recent statistics from the EU, the number of people living in seismic areas increased by 93% from 1.4 billion in 1975 to 2.7 billion in 2015 [3]. Similarly, United States Geological Survey (USGS) study indicates almost half of the population in US is exposed to potentially damaging ground shaking from earthquakes [4]. In light of the above, relocating the entirety of the potentially affected population to mitigate the risk is not practical. Engineers must be able to make informed decisions regarding the behaviour of liquefiable soils, and it is imperative that the range of soil behaviour is well understood before embarking on detailed designs in liquefaction prone areas.

2.2   Soil mechanics concepts and definitions

This section is intended for readers who are unfamiliar with geotechnics. It provides an introduction to some of the terms and concepts necessary for understanding the liquefaction phenomenon. Italics are used to indicate terms used frequently hereafter.

In saturated soils, there are two loadpaths supporting the applied stresses: (a) forces acting between the grains of solid material, and (b) pressure in the water in the gaps between the grains. These may be treated as an *effective stress* in the *soil skeleton* acting in parallel with *pore pressure* in the water (Terzaghi's concept of effective stress). The *total stress* (which reacts the external load) is the sum of the effective stress and the pore pressure. In the long-term equilibrium condition, the pore pressure tends to follow a hydrostatic distribution, increasing by 10 kPa per metre of depth, while the effective stress supports the buoyant weight of the soil. However, the same external load can potentially be supported by different combinations of pore pressure and effective stress: for example, reduced effective stress plus increased pore pressure. The difference between the actual pore pressure and the hydrostatic pore pressure is termed *excess pore pressure*. Gradients of excess pore pressure drive water to seep away through the soil until, after some time has passed, the hydrostatic pressure distribution is restored – a process known as *consolidation*. In some experiments on small soil samples, seepage from the sample is prevented (for example by a rubber membrane) – these are described as *undrained*.

Sandy soils exhibit pressure-dependent shear strength and stiffness. When the soil is saturated, it is the effective pressure (i.e. the pressure in the soil skeleton, not the total pressure) that determines shear strength. Thus, if the proportion of the external load carried by effective stress changes, then the shear strength also changes. Shear strength is commonly described in terms of a friction angle, i.e. a multiple on effective pressure or normal stress. Because of the proportionality between shear strength and pressure, it is convenient to describe constitutive models in terms of *stress ratio*, which may be thought of as shear stress divided by effective pressure.

When sandy soils are subject to shear strains, the packing arrangement of the grains changes, causing volumetric change of the soil skeleton as illustrated in Figure 2. Loose sands exhibit predominantly contractive behaviour – shear strains cause the grains to align such that they could potentially be packed into a smaller space. Thus, when saturated loose sands are subjected to undrained monotonic shearing, the effective pressure reduces (leading to reduction of shear stiffness and strength) together with generation of excess pore pressure. Dense sandy soils initially exhibit contractive behaviour but then dilate, leading to increase of stiffness and strength while the pore pressure reduces. These changes of

effective pressure and pore pressure can accumulate when the soil is subject to cyclic shearing. Volumetric change of the soil skeleton ceases at large shear strains when the soil reaches the so-called *Critical State* (a relative density that is not altered by further shearing), as indicated in the right-hand diagram of Figure 2.
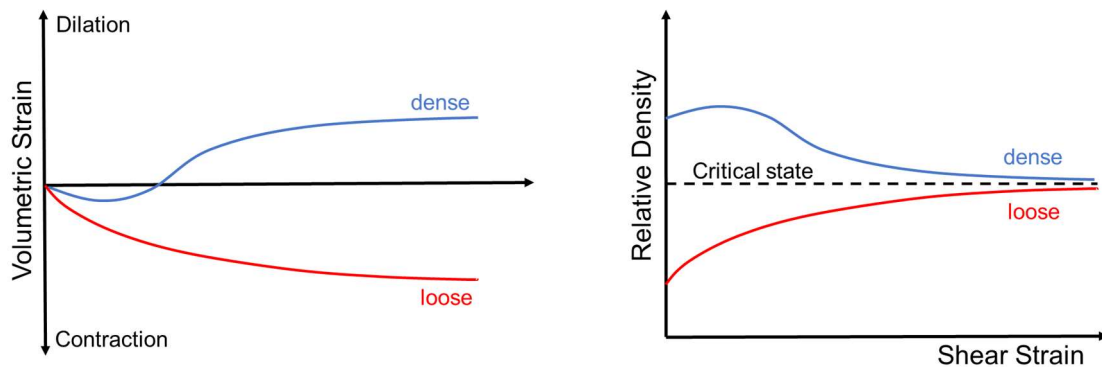

Fig.2:   Dilation/contraction behaviour of dense and loose sands during shearing, in terms of volumetric strain (left) and relative density (right)

2.3   Cause of liquefaction

The process by which liquefaction occurs is illustrated diagrammatically in Figure 3 for a sandy soil with a low initial relative density. The left-hand diagram represents the state before the earthquake. The externally-applied vertical stress σ is carried partly by contact forces between the soil grains (*effective stress*) and partly by pressure in the water (*pore pressure*). The soil exhibits shear stiffness and strength because of friction between the grains.

During the earthquake (middle diagram in Figure 3) the soil is subject to shear loading. The soil skeleton contracts, i.e., the grains realign such that they could potentially be packed into a smaller space. The total volume of water and soil grains is unchanged, but the soil grains no longer carry any vertical load - the effective stress has fallen to zero. All of the externally-applied stress is now reacted by the pore pressure (*pore pressure generation).* The soil is in a liquefied state and behaves like a quicksand.

After the earthquake (right-hand diagram in Figure 3), the increased pore pressure drives water to seep away through the soil (*pore pressure dissipation*) until the contact force between the grains, and therefore also the stiffness and strength of the soil, are restored and the pore pressure returns to its initial value (right-hand diagram).
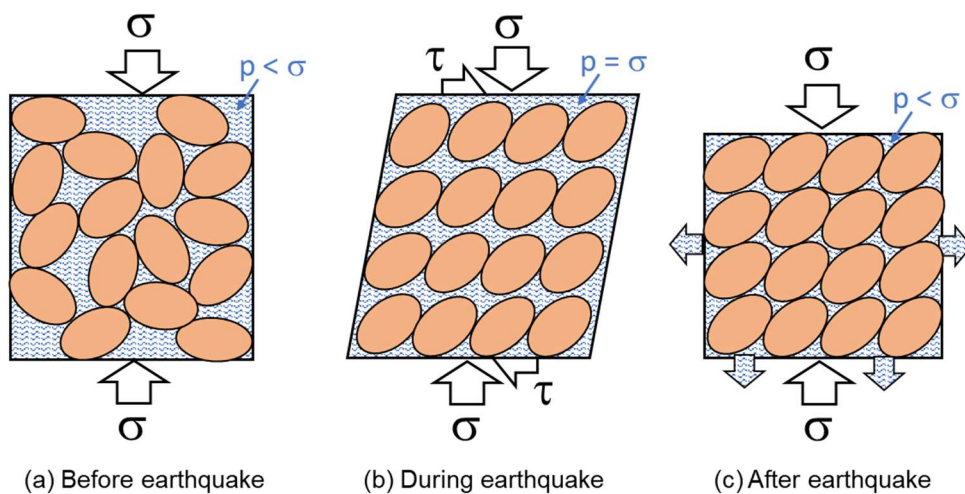

(a) Before earthquake   (b) During earthquake   (c) After earthquake

Fig.3:   Diagrammatic illustration of liquefaction

The essential requirements for simulation of liquefaction during earthquakes are therefore (a) a soil material model that exhibits realistic cyclic shear response together with the accompanying volumetric changes of the soil skeleton; and (b) suitable treatment of the pore water including separation of the pore pressure from the effective stress and modelling of seepage and consolidation. Section 3 describes how these are achieved in LS-DYNA.

2.4 The challenge of modelling liquefaction in real situations

The first task is to mimic simple laboratory tests on shearing of undrained sands in which the boundary conditions can be reasonably well controlled. Often, especially with dense sands, laboratory specimens can fail prematurely due to poor preparation techniques and sometimes due to adverse particle rearrangement in the early stages of shearing. Consequently, careful selection of tests, preferably from well-documented sands of consistent mineralogy, to enable numerical verisimilitude is required.

Having developed a reasonable numerical model that can mimic laboratory scale tests, we can move to the simulation of 3D situations. Here the volume of sands participating in the shearing event is orders of magnitude larger than in the laboratory. The in-situ state of stress and variations in void ratio will vary from those in the laboratory and the soil will exhibit the effects of aging and pre-shearing that are absent in reconstructed sand samples in the laboratory. In real loading situations, the sand may form shear bands that are not replicated in the laboratory and the intra-cycle drainage conditions in the various parts of the stress field can lead to more or, occasionally, less tendency towards liquefaction.

Engineers who are considering a real situation will therefore generally be seeking a numerical model that provides a cautious estimate of the potential for liquefaction, such that mitigation strategies can be implemented.

3 LS-DYNA modelling of liquefaction

3.1 Pore water modelling

Pore water is modelled in LS-DYNA following the effective stress concept of Terzaghi, whereby pore pressure acts in parallel with the effective stress. The effective stresses are simply the stresses calculated by the selected LS-DYNA constitutive model in the normal way. The input properties on the `*MAT` cards relate only to the effective stress behaviour; the only property influenced by the presence of water is the density, which should be given as the density of the soil/water mixture. Pore pressure, treated as a nodal variable, is calculated separately, interpolated onto the elements to calculate the element pore pressure which is added to the effective stresses from the constitutive model to give the total stress, from which the element internal forces are computed. Thus, the pore water treatment is independent of which constitutive model is used and the constitutive model does not require information regarding the pore water. Pore water behaviour and properties are given on `*CONTROL_PORE_FLUID`, `*BOUNDARY_PORE_FLUID`, and `*MAT_ADD_PERMEABILITY`, while the initial pore pressure profile is specified with `*INITIAL_PWP_DEPTH`.

Note that both the effective stress and the pore pressure are applied to the full area of the element (and not to the respective areas of soil grains and water). Although it may seem counter-intuitive that both soil grains and water are apparently considered to occupy the same space, this is a commonly adopted concept in geotechnics, and the values of input properties such as the permeability are adapted to suit this method.

The pore pressure analysis type is set by the user on a per-part basis using the input variables ATYPE (constant value) or ACURVE (analysis type switching as a function of time during the analysis) and can take values with the following meanings:
1. *Undrained*: water is trapped within each element and pore pressure develops via a user-supplied bulk modulus in response to volumetric strains. Used to represent the effect of rapid changes of load, often in relatively impermeable soils such as clays. In the context of liquefaction studies, this analysis type is used to model small-scale calibration experiments such as undrained triaxial or direct shear tests in which the specimen is saturated and there is no way for the water to escape. Under these conditions, pore pressure generation will be modelled but not pore pressure dissipation.
2. *Drained*: pore pressure is hydrostatic, or other distribution defined by the user (for example via *INITIAL_PWP_DEPTH). Represents the situation where the applied loading has remained constant

for sufficient time for any excess pore pressure to drain away, wholly or partially. This analysis type may be used while applying long-term loading in order to reach the pre-earthquake stress state.

3. *Time-dependent consolidation*: as for the undrained case, pore pressure develops via a user-supplied bulk modulus in response to volumetric strains, but excess pore pressure gradients drive pore water seepage according to Darcy's law (below), and nett changes of water volume arising from the seepage flows lead to changes of pore pressure.

$$v_{seep} = -\kappa\nabla(^{p}/_{\rho g} + z)$$

Where v_{seep} is the seepage velocity (taken as the volume flow rate per unit cross-sectional area of the soil/water mixture), κ is the permeability in units of length/time given on ***MAT ADD PERMEABILITY**, p is pore pressure, ρ is water density, g is the acceleration due to gravity, and z is the z-coordinate. The model's global z-axis is assumed to be vertically upwards. This analysis type is applied during and after the earthquake motion to enable generation and dissipation of pore pressure. It can also be used to simulate the comparatively slower cyclic wave, icepack or ship impact loading in offshore situations.

4. *Steady-state consolidation*: a variant of time-dependent consolidation used to find the long-term condition after consolidation has occurred; not used in the analyses presented herein.

3.2   Constitutive model: SANISAND

The search for a theoretical basis from which the results of experiments on sandy soils may be predicted from macro-level inputs (such as stress state, relative density and loading history) has occupied researchers for the last several decades. Several research efforts have focused on SANISAND (Simple ANIsotropic SAND plasticity model), a family of soil constitutive models based on bounding surface plasticity and Critical State soil mechanics dating back to the 1990s. SANISAND is essentially a framework onto which different authors have added different features. Dafalias and Manzari (2004) [5] provide a good introduction to "classic" SANISAND together with the necessary equations for a full 3D implementation. This paper is referred to hereinafter as *D&M2004* for brevity. Further developments and improvements continue to be published, for example PM4SAND described by Boulanger & Ziotopoulou [6], and the memory-surface model of Yang, Taiebat and Dafalias (2021) [7].

A SANISAND material model has been developed for LS-DYNA based largely on D&M2004 with minor additional features from other sources. The key points of the model may be summarised briefly as follows. Some of these points are illustrated in Figures 4 and 5. The equations are not given here but may be found in D&M2004.

The main state variables are:
- *Stress ratio*, which in principle is shear stress divided by pressure and may be visualised in the left-hand diagram of Figure 4 as the angle of a line from the origin to a given stress state. Although that description implies a two-dimensional model with stress ratio being a scalar quantity, the model is written for 3D multiaxial applications and the stress ratios are in fact tensors (deviatoric stress tensor divided by pressure) – see D&M2004 for further details.
- *Void ratio*, e, which is a measure of how tightly packed the grains are (lower void ratio means more tightly packed). The initial void ratio is given in the input data, and thereafter the void ratio varies with contraction/dilation history. Void ratio has a linear relationship with relative density.

The governing principles of the shear response are:
- Only changes of stress ratio can cause plastic shear strain.
- A bounding surface (labelled in Figure 4) defines the upper limit stress ratio. This can be considered as the failure surface.
- There is a small conical yield surface (labelled "elastic region" in Figure 4) centred on a back stress ratio which is continuously updated to follow the stress path. On reversal of loading, the stress state passes through the small elastic zone before nonlinear behaviour recommences in the reverse direction.
- Hardening modulus (defined in terms of stress ratio) is a function of the "distance to the bounding surface" such that hardening reduces smoothly to zero as the stress ratio approaches the bounding surface, for example at point B in Figure 4. Note that the aim point on the bounding surface depends on loading direction.
- The cyclic shear stress-strain response at constant effective pressure is shown in the right-hand diagram of Figure 4.

- The shear response is also influenced by Lode angle: in the deviatoric plane the various surfaces are non-circular.
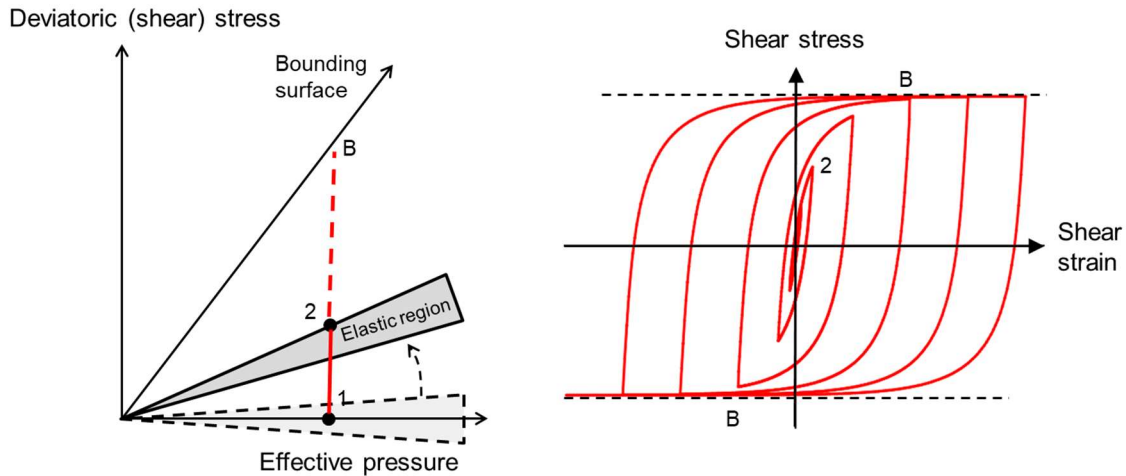

Fig.4: *Schematic of SANISAND yield surface and bounding surface (left) and cyclic shear stress-strain response at constant effective pressure (right)*

Dilation and contraction response operates in the following manner:
- Volumetric strain increment is the product of plastic strain increment with a variable dilation angle D.
- D is negative, i.e. contractive, at stress ratios below the dilatancy surface (yellow zone in Figure 5) and positive, i.e. dilative, above it (purple zone in Figure 5), and in general is a continuous function of the stress ratio "distance to the dilatancy surface" such it that changes from negative to positive at the dilatancy surface, for example at the point labelled 2 in Figure 5.
- Volumetric behaviour is influenced by several other quantities, including Lode angle, and the model includes "fabric change" during the dilation phase that increases the subsequent tendency to contract upon reversal of loading.

The critical state is implemented in the model as follows:
- State parameter ψ is used to express the "distance from the critical state". It is given by $\psi = e - e_c$ where e is the current void ratio, e_c is the void ratio in the critical state, and e_c is a function of pressure.
- Both the dilatancy surface and the bounding surface vary with ψ such that when the material is in the critical state, i.e. $\psi=0$, the dilatancy and bounding stress ratios coincide on the line marked CSL in Figure 5. The distance to the dilatancy surface is then zero, meaning that $D = 0$ and shearing does not cause any further volume change.
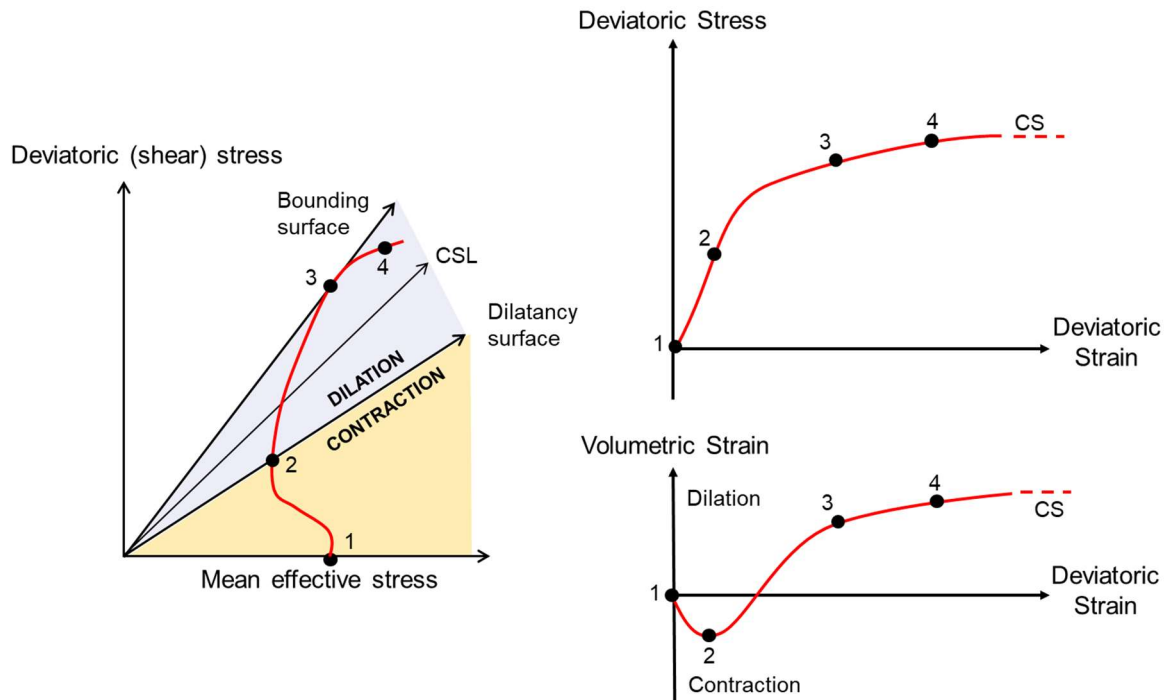
Fig.5: *Schematic of SANISAND volumetric behaviour showing a stress path for undrained monotonic shear (left), together with stress-strain and volumetric strain versus deviatoric strain relationships for the same stress path (right)*

The model also includes options for inherent anisotropy effects based on Dafalias, Papadimitiou and Xiang [8] and for closed-ended yield surface representing grain crushing based on Taiebat and Dafalias [9], but since neither of those capabilities were invoked in the examples presented herein, they will not be described further.

While the basic principles of SANISAND as expressed in D&M2004 are widely accepted, the model does have certain weaknesses that recent research seeks to address – for example, it can be calibrated to match cyclic undrained laboratory tests at a particular stress ratio, but if a similar test is then conducted at a different stress ratio the D&M2004 results are shown to be less sensitive to stress ratio than real soils. These weaknesses have been a focus for more recent study, see for example PM4SAND described by Boulanger & Ziotopoulou [6], and Yang, Taiebat and Dafalias [7]. Work such as this will likely form the basis of future improvements to the LS-DYNA material model.

It is expected that either this material model, or a further development of it, will be released in a future version of LS-DYNA.

3.3 Example undrained cyclic shear analysis

Figure 6 shows results from an example analysis in which a single element is subjected to load-controlled cyclic shearing under undrained pore water conditions. The applied load is a shear stress varying sinusoidally with a constant amplitude of 10 kPa, while a 100 kPa non-time-varying direct stress is applied along all three global axes. The pore pressure analysis type is set to undrained. As shown in the right-hand graph, excess pore pressure is generated (black line) while the effective pressure (blue line) reduces.
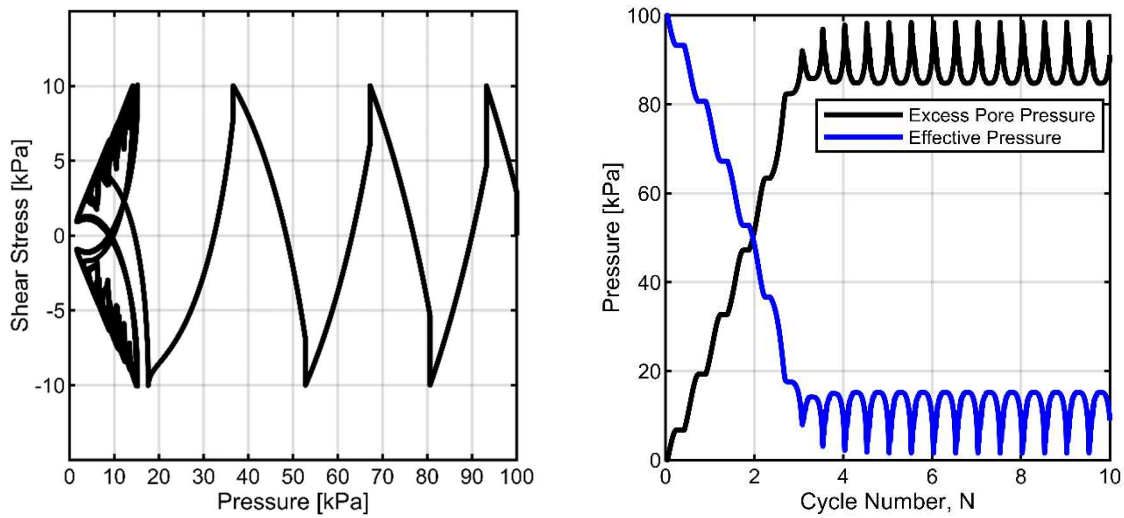
Fig.6:   Results from example analysis of cyclic shear test with LS-DYNA SANISAND material model. Left: shear stress versus pressure; right: effective pressure and excess pore pressure time-histories.

4   Calibration of SANISAND model

Material properties have been calibrated against undrained monotonic and cyclic direct simple shear tests by Bastidas [10] on Ottawa F-65 sand. This particular sand is used in the large-scale testing exercise which will be elaborated in the Section 5 of this paper. Figure 7 illustrates the results of the calibration exercise undertaken for a series of monotonic direct shear tests on Ottawa F-65 sand with different relative densities. As can be seen in Figure 7, there is reasonably good agreement between the results of the physical tests and the outputs of the LS-DYNA model.
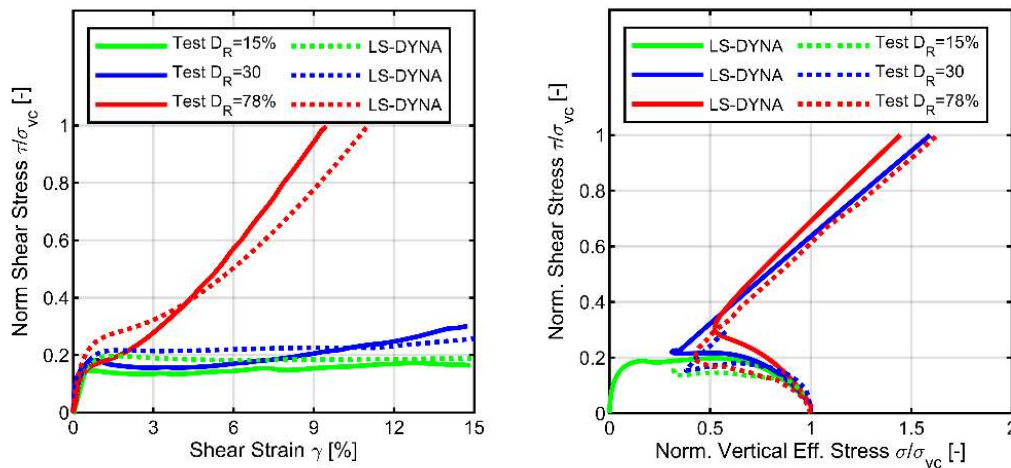

Fig.7:   Comparison of the physical and numerical element test results under monotonic loading. Left: Normalized shear stress versus shear strain plot; right: normalized shear stress versus normalized effective stress plot.

Example results for the cyclic loading case are illustrated in Figure 8 for the case of Ottawa F-65 sand at a relative density (D_r) of 39% and a CSR (Cyclic Stress Ratio) of 0.1. The LS-DYNA model reaches a liquefied state after two cycles whereas in the experiment the same state is reached after four cycles, but such differences are likely to lie within the spread of test-to-test variability.
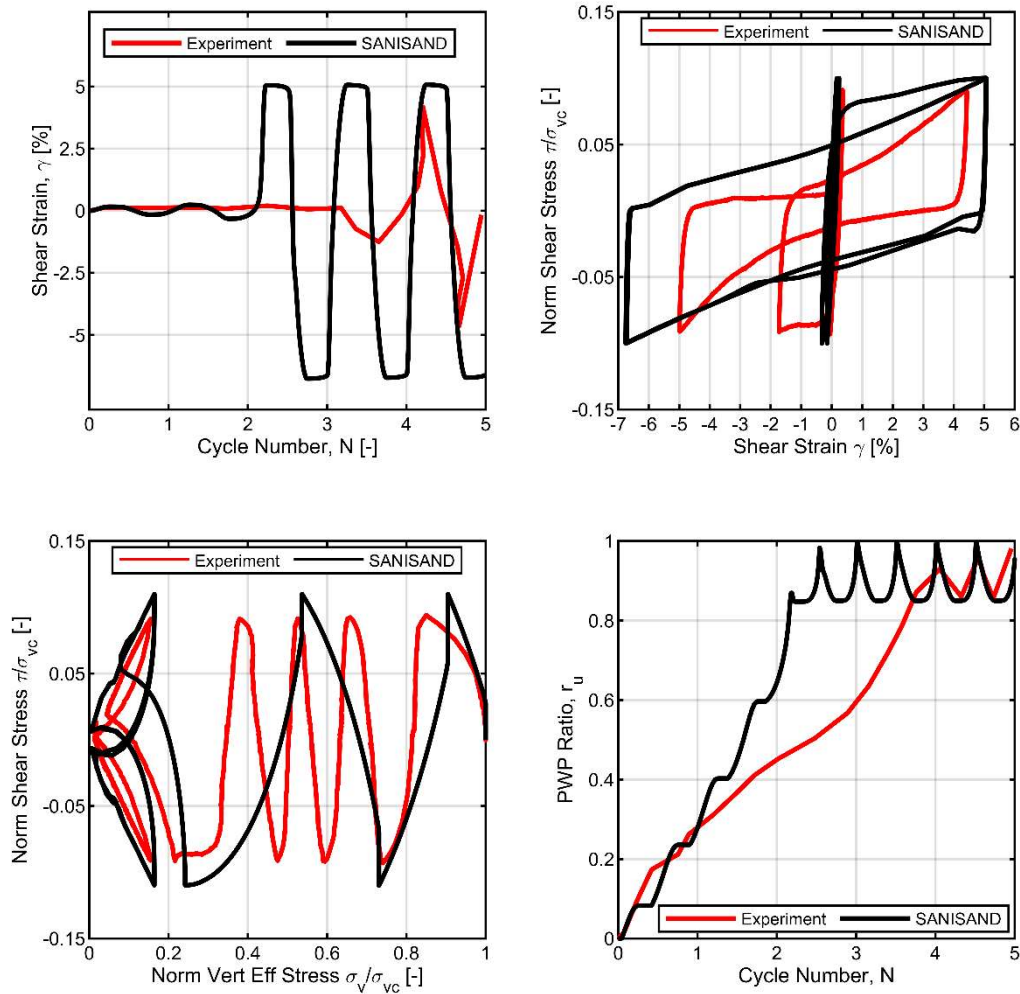
Fig.8: Comparison of physical and numerical element tests' results for Ottawa F-65 sand at a confining stress of 100 kPa

In total, 4 experiments were used in calibrating the input data for different relative densities of Ottawa sand as summarised in Table 1. The test identification numbers indicated in the first column of Table 1 follow on from the naming convention used by Bastidas [10]. The number of cycles to achieve liquefaction is based on the r_u = 0.9 criterion where r_u or pore water pressure ratio is defined as the ratio of the pore pressure to the normal stress (in these cases, 100 kPa).

Table 1: List of the calibration runs undertaken with different soil initial conditions

Bastidas Test ID*	CSR	Initial Void Ratio	Relative Density (%)	Confining Stress (kPa)	Number of Cycles to Liquefy	
					LS-DYNA	Lab. Tests
17	0.1	0.7052	39	100	2	3
6	0.11	0.6956	42	100	2	3
23	0.16	0.5836	77	100	2	3
68	0.21	0.5964	73	100	2	2

*ID or test number of the cyclic shear tests reported in Bastidas (2016)

5   Simulation of shake table experiment

Several experimental programmes and research initiatives have attempted to shed light on the liquefaction phenomena. Given the vast uncertainty of the onsite soils and the inherently chaotic nature of the earthquake excitations, different research consortiums have held blind-prediction contests where

laboratory tests with controlled soil profiles and loading regimes were employed with the incentive being the improvement of existing numerical tools. For instance, verification of Liquefaction Analysis by Centrifuge Studies (VELACS) [11] and Liquefaction Experiments and analysis Projects (LEAP) [12] studies were undertaken where a uniform layer of sand was used to study the liquefaction response and numerical models' findings were compared to experimental results.

Similar to the research initiatives mentioned above, a series of large-scale shake table tests were conducted at the shake table facility at the University of California, San Diego (Powell Laboratory) in June 2018 to evaluate the effects of liquefaction induced settlement on shallow foundations [13]. In this section of the paper, the details of the experimental model and the comparison of the physical tests with an LS-DYNA model will be elaborated. The experiment was conceived as part of a blind prediction contest in which the participants were asked to estimate the settlement in advance of the experiment taking place. The LS-DYNA model reported here formed part of that blind prediction exercise.

5.1 Experiment set-up

The laminar box assembly and a sketch of the instrumentation used in the experiments are illustrated in Figure 9. The laminar box with the internal dimensions of 3.9 × 1.8 × 2.9 m [length × width × height] housed the three-layer soil model. Specifically, the soil layers consisted of an unsaturated top layer (medium dense sand) and a basal saturated dense sand layer. A saturated loose sand layer was deliberately placed in between these layers to achieve liquefaction during the application of the base excitations. The laminar box consists of a series of rectangular frames stacked on top of each other. Each frame can slide horizontally relative to the frames above and below such that the box itself has a low shear stiffness but still contains the soil horizontally. A membrane liner prevents escape of water or soil. A concrete foundation block was introduced in the upper medium dense sand layer and steel weights were placed above the foundation to represent the weight of the model structure.
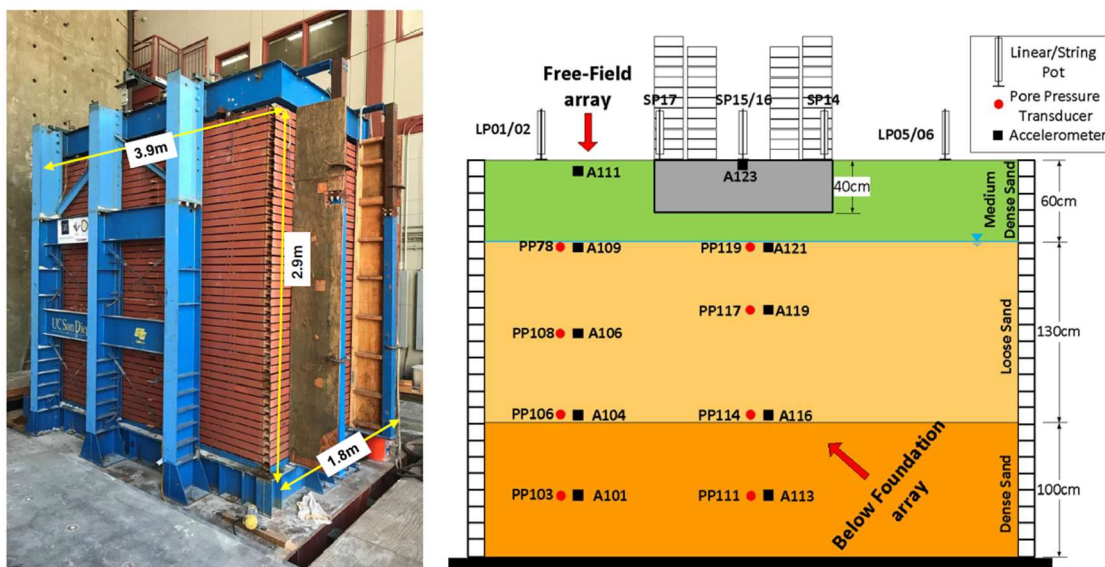

Fig.9:   Photograph depicting the laminar soil container and a cross-section illustrating some of the instrumentation employed in the tests at UC San Diego Powell Laboratory [13]

Ottawa F-65 sand was used throughout the experimental programme and interested readers are referred to the work of Bastidas [10] for detailed engineering properties of this material. In order to achieve different material densities, the compactive effort was varied. The relative densities (D_r) of the medium dense sand, loose sand, and dense sand materials varied between 50-55, 40-45, and 85-90%, respectively.

Although the experimental programme made use of different loading regimes, this paper will focus on the results of input excitation designated as Shake 1-1 [13]. Shake 1-1 input motion applied to the shake table test is illustrated in Figure 10. The predominant frequency of the input is 2 Hz with a 6 s ramp on the onset followed by a 6 s constant amplitude before tapering off for 3 s. The recording of the sensor data was continued until 80 s from the start of the shaking to capture the dissipation behaviour of the

excess pore water pressures and more importantly, the residual settlement behaviour of the model foundation and the free-field ground.
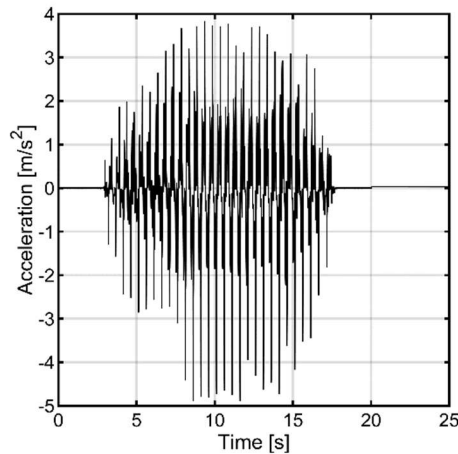

Fig.10: Input base excitation applied in the shake table tests

5.2   LS-DYNA model

The LS-DYNA model of the experiment is illustrated in Figure 11. The method of analysis follows the Direct Method as described by Bollisetti and Whitaker [14]. Gravitational loads are explicitly included and the four loading stacks are modelled as columns so that any inertial effects arising from the chosen arrangement are included in the foundation behaviour and soil response. Likewise, the box frames (modelled with rigid beam elements) and perimeter membrane (shell elements) are explicitly modelled, with an interface friction of 0.4 for the frames and zero for the membrane. The lowest frame was fully fixed to the shaking table. Initially, the water table was modelled at the interface of the medium dense and loose sand layers at a depth of 0.6m.

Apart from the top-most layer, the sand layers were modelled using the SANISAND material model described in previous sections of this paper and calibrated as described in Section 4.
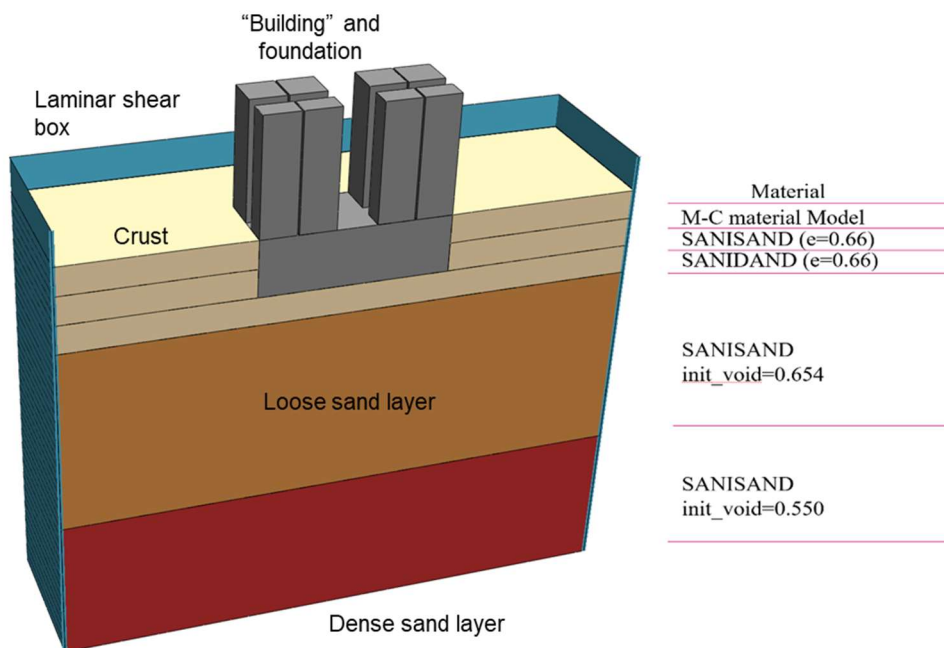

Fig.11: Left: Isometric cut-away view of the 3D LS-DYNA model; right: soil layers utilized in the model

5.3   Results

Images comparing the situation shortly after the experiment with the LS-DYNA model are shown in Figure 12. The loose sand layer liquefies during ground motion, resulting in the "building" (as represented by the concrete foundation block with towers of weights above) settling more than 250mm and visibly sinking into the sand. The simulation was terminated at the end of the ground motion due to extreme deformation of the Lagrangian mesh around the foundation. That issue is unlikely to be problematic for analyses of real-life designs – if such extreme settlements were predicted, then the design of the structure would in any case need to be revised.
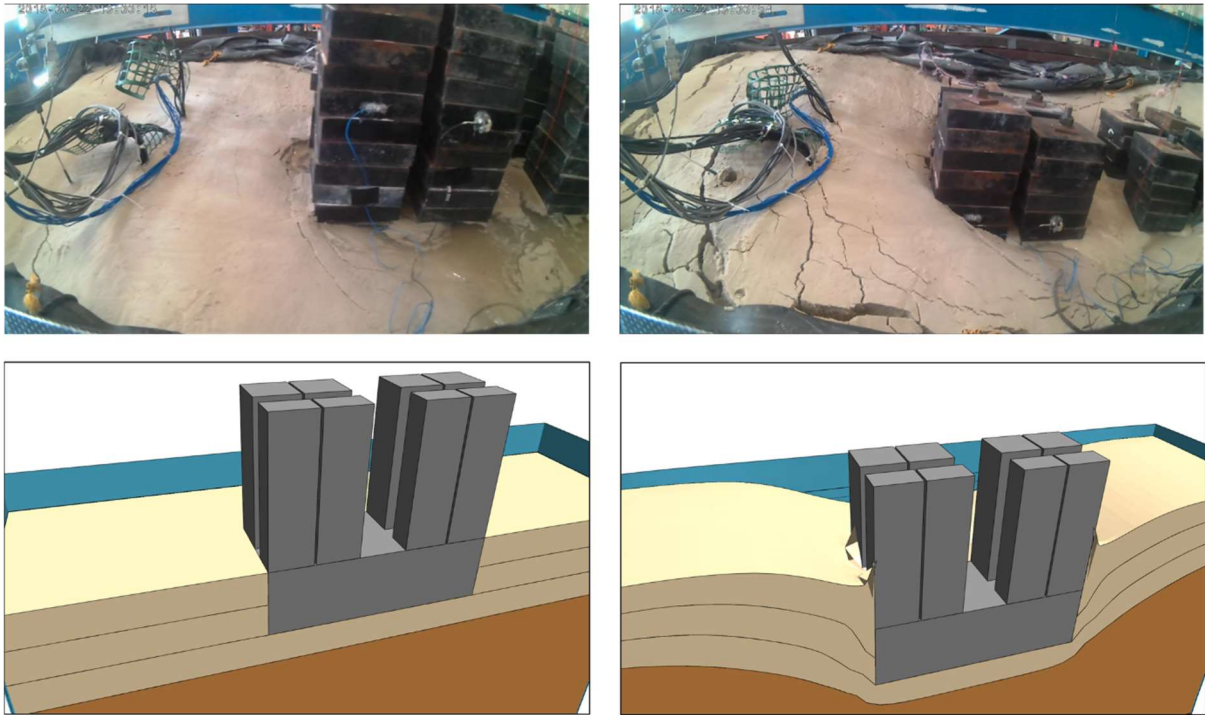

Fig.12: Experiment and LS-DYNA model (cut-away view). Left: before ground motion. Right: after ground motion. (Video stills from Motamed (2018) Personal communication)

The settlement predictions at locations indicated in Figure 13 are compared to the experimental results as reported by Orang et al. (2021) [13] in Figure 14. Positive settlements are towards the base of the model. On the foundation (locations marked FD), the settlements predicted by the LS-DYNA model (around 350 mm) are about 25% greater than in the experiment (around 280 mm), and occur more rapidly. However, this may be considered a reasonably favourable result given the spatial variability of soils and uncertainties in the material input data: for example, the shear stiffness of the laminar box was unknown, and calibration data for the Ottawa sand was available only at confining pressures of around 50-100kPa while in the experiment the confining pressure is around 10-20kPa. Furthermore, if used for design purposes, this analysis would be pragmatically conservative, i.e. leading to safer designs.

In the free-field (FF) locations the settlements are predominantly negative which means that the displacements are upwards (heave); this results from the soil from under the settling foundation being displaced within the confined space of the laminar box.
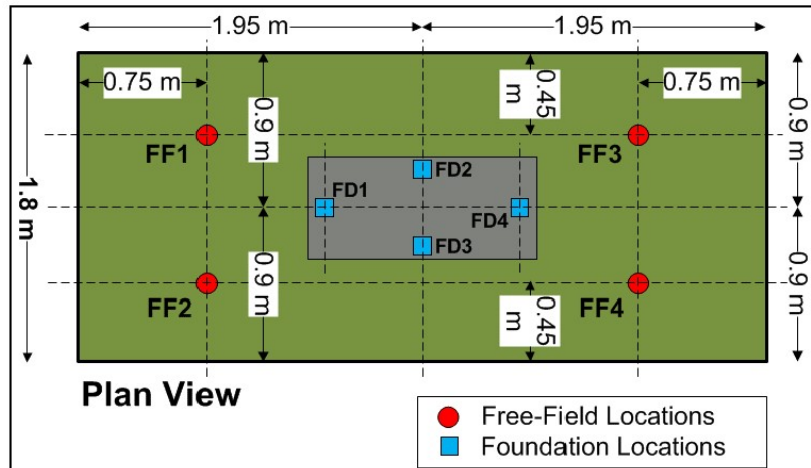
Fig.13: Sketch illustrating the settlement prediction locations on the topmost plane of the soil surface placed in the laminar box assembly.
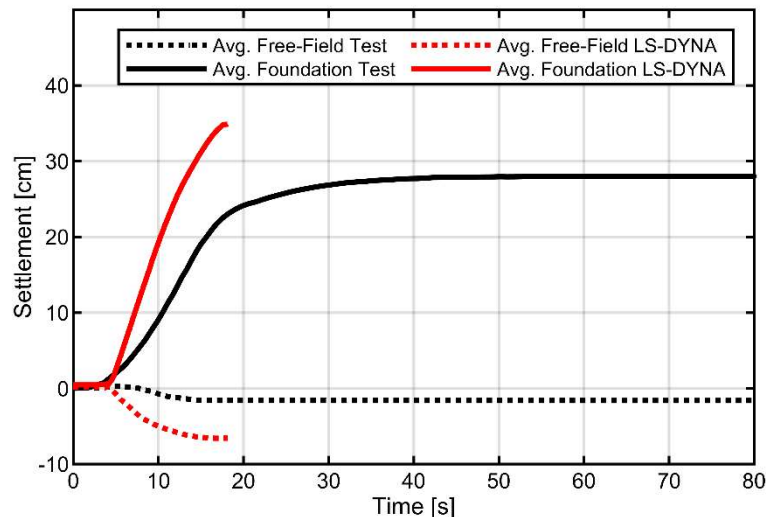

Fig.14: Settlement time-histories for laboratory test and LS-DYNA model

6   Example application – offshore wind turbine foundation

Offshore wind turbines are now being constructed in seismically-active regions and it is not always possible to avoid liquefiable sand layers. The objective is then to design the foundation to accommodate liquefaction without unacceptable settlements or rotations and without exceeding the load capacity of the structure, for example by providing a large monopile driven through the liquefiable layer and sufficiently deep into denser soil beneath. Figure 15 shows an LS-DYNA model of this situation. The tower above the seafloor is modelled with beam, mass and inertia elements. The monopile is modelled with shell elements and the soil with solid elements, both inside and outside the monopile. The dense sand layers are modelled with ***MAT_HYSTERETIC_SOIL** while the loose sand layer uses the SANISAND material model described in this paper.

As shown in Figure 15, pore pressure generation is predicted in the loose sand layer together with large shear strains. Hence, the model is capable of capturing both the inertial loads from the wind turbine and the kinematic loads from the deforming soil. Moreover, permanent rotations and the stability of the structure can be assessed at the end of shaking.
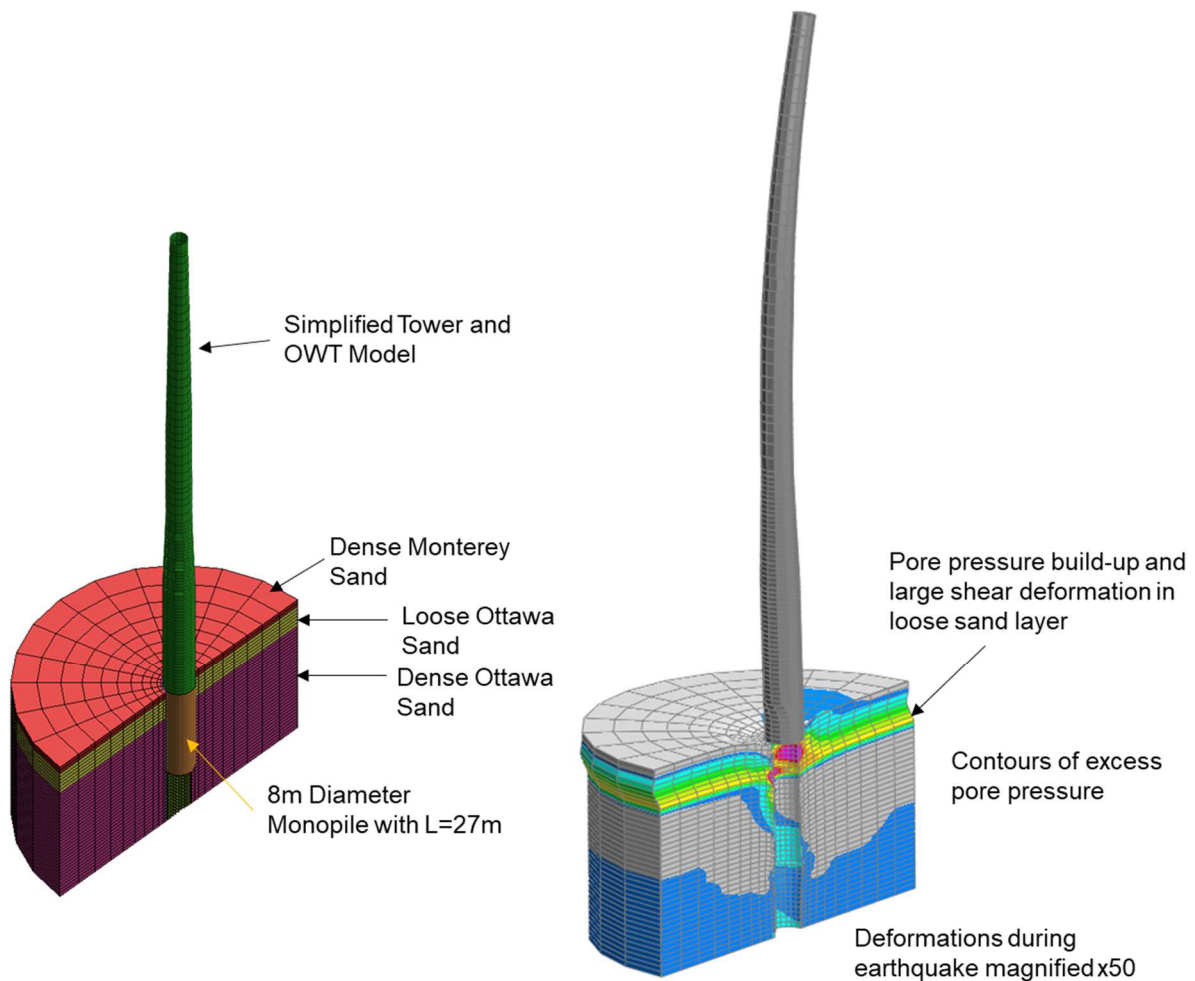
Fig.15: Cut-away views of LS-DYNA model of offshore wind turbine foundation with liquefiable loose sand layer

7   Future outlook

Further developments of the SANISAND material model will address known shortcomings of the D&M2004 model. In particular, experiments indicate a greater sensitivity of liquefaction to cyclic stress ratio than is shown by the SANISAND model. In other words, the model can be calibrated to give realistic results at one cyclic stress ratio, but then lower cyclic stress ratios than used in the calibration tests tend to produce conservative predictions of liquefaction in the LS-DYNA model that might not occur in reality, leading to higher loads on the structure. This is not necessarily problematic in the design of structures, where conservative predictions lead to safer designs, but could in some instances lead to opportunities for cost-saving being missed.

The SANISAND material model will be made available in a future release of LS-DYNA.

8   Summary

Liquefaction is a phenomenon occurring in loose sandy saturated soils during earthquakes, which can potentially result in catastrophic damage to structures. Designers of structures on sites with liquefiable soil layers must consider the effect of liquefaction on the structure.

To analyse these complex problems requires a finite element program that has well-developed nonlinear, 3D capabilities for structures and soils; fast turn-around time even for big 3D models; the ability to model pore water pressure; and a constitutive model that captures the contracting and dilating behaviours of sandy soils when subject to shear strains. The development of a suitable constitutive

model for this application, described in this paper, is the final "piece in the jig-saw" enabling the power of LS-DYNA to be directed towards designing structures in these challenging environments.

The model displays the behaviours shown in experiments. It tends to produce conservative results which are useful in the context of engineering design. Further developments are planned around the accuracy of predictions of liquefaction. The material model will be included in a future release of LS-DYNA.

9   Literature

[1] Tokimatsu, K., Kojima, H., Kuwayama, S., Abe, A. and Midorikawa, S., 1994. Liquefaction-Induced Damage to Buildings in 1990 Luzon Earthquake. Journal of Geotechnical Engineering, 120(2), pp.290-307.

[2] Sumer, B., Ansal, A., Cetin, K., Damgaard, J., Gunbak, A., Hansen, N., Sawicki, A., Synolakis, C., Yalciner, A., Yuksel, Y. and Zen, K., 2007. Earthquake-Induced Liquefaction around Marine Structures. Journal of Waterway, Port, Coastal, and Ocean Engineering, 133(1), pp.55-82.

[3] EU Science Hub - European Commission. 2021. Atlas of the Human Planet 2017 – how exposed are we to natural hazards? - EU Science Hub - European Commission. [online] Available at: <https://ec.europa.eu/jrc/en/news/atlas-human-planet-2017-how-exposed-are-we-natural-hazards> [Accessed 1 September 2021].

[4] Usgs.gov. 2021. Nearly Half of Americans Exposed to Potentially Damaging Earthquakes. [online] Available at: <https://www.usgs.gov/news/nearly-half-americans-exposed-potentially-damaging-earthquakes> [Accessed 1 September 2021].

[5] Dafalias, Y.F. & Manzari, M.T.: "Simple plasticity sand model accounting for fabric change effects", Journal of Engineering Mechanics, 2004 130(6), 622–634.

[6] Boulanger R. W., Ziotopoulou K. PM4SAND (Version3): A sand model for earthquake engineering applications, Report No. UCD/CGM-15/01, UC Davis, 2015

[7] Yang M., Taiebat, M., and Dafalias Y.F., A New Sand Constitutive Model for Pre- and Post-liquefaction Stages. ICAMAG 2021

[8] Dafalias, Y.F., Papadimitriou, A. G., and Li, X. S. (2004). "Sand plasticity model accounting for inherent fabric anisotropy." Journal of Engineering Mechanics,130(11), 1319–1333.
.
[9] Taiebat, M., and Dafalias Y.F., SANISAND: Simple anisotropic sand plasticity model. Int. J. Numer. Anal. Meth. Geomech. 2008; 32:915–948

[10] Bastidas, A. M. P. 2016. "Ottawa F-65 sand characterization." Ph.D. dissertation, Dept. of Civil and Environmental Engineering, Univ. Of California, Davis.

[11] Arulanandan, K., and R. F. Scott. 1993. "Verification of numerical procedures for the analysis of soil liquefaction problems. Vol. 1: Experimental results and numerical predictions." In Proc., Int. Conf. on the Verification of Numerical Procedures for the Analysis of Soil Liquefaction Problems. Rotterdam, Netherlands: A.A. Balkema.

[12] Kutter, B. L., T. J. Carey, T. Hashimoto, M. T. Manzari, A. Vasko, M. Zeghal, and R. J. Armstrong. 2015. "LEAP database for verification, validation, and calibration of codes for simulation of liquefaction." In Proc., 6th Int. Conf. on Earthquake Geotechnical Engineering. Christchurch, New Zealand: International Society for Soil Mechanics and Geotechnical Engineering.

[13] Jahed Orang, M., Motamed, R., Prabhakaran, A. and Elgamal, A., 2021. Large-Scale Shake Table Tests on a Shallow Foundation in Liquefiable Soils. Journal of Geotechnical and Geoenvironmental Engineering, 147(1), p.04020152.

[14] Bolisetti C and Whitaker AS (2015) Site response, soil-structure interaction and structure soil-structure interaction for performance assessment of buildings and nuclear structures. MCEER-15-0002. Technical report under NSF grant# CMMI-0830331, 388pp